ADVANCING EARTH AND SPACE SCIENCES

Geophysical Research Letters

RESEARCH LETTER
10.1029/2024GL113199

Key Points:
- Tropical cyclones (TCs) contribute approximately 30% of annual maximum discharge, highlighting their substantial role in flood generation
- TCs emerge as the dominant driver of extreme floods with long return periods
- The spatial changes of TC-induced discharge correlated strongly with changes in TC tracks and associated precipitation

Supporting Information:
Supporting Information may be found in the online version of this article.

Correspondence to:
J. Liu,
junguo.liu@gmail.com

Citation:
Chen, A., Wang, J., Toumi, R., Huang, H., Yang, L., Chen, D., et al. (2025). Impact of tropical cyclone precipitation on fluvial discharge in the Lancang–Mekong River Basin. *Geophysical Research Letters*, *52*, e2024GL113199. https://doi.org/10.1029/2024GL113199

Received 28 OCT 2024
Accepted 6 APR 2025

Author Contributions:
Conceptualization: Aifang Chen
Formal analysis: Aifang Chen, Ralf Toumi, Hao Huang
Funding acquisition: Deliang Chen, Junguo Liu
Investigation: Aifang Chen, Deliang Chen, Junguo Liu
Methodology: Aifang Chen, Jie Wang
Supervision: Junguo Liu
Validation: Jie Wang, Ralf Toumi, Long Yang, Deliang Chen, Bin He
Visualization: Aifang Chen, Jie Wang, Hao Huang, Long Yang, Deliang Chen, Bin He
Writing – original draft: Aifang Chen
Writing – review & editing: Aifang Chen, Jie Wang, Ralf Toumi,

Impact of Tropical Cyclone Precipitation on Fluvial Discharge in the Lancang–Mekong River Basin

Aifang Chen[1,2], Jie Wang[3], Ralf Toumi[4], Hao Huang[2], Long Yang[5], Deliang Chen[6], Bin He[7], and Junguo Liu[8]

[1]School of Environment and Civil Engineering, Dongguan University of Technology, Dongguan, China, [2]School of Environmental Science and Engineering, Southern University of Science and Technology, Shenzhen, China, [3]College of Earth and Environmental Sciences, Lanzhou University, Lanzhou, China, [4]Department of Physics, Imperial College London, London, UK, [5]School of Geography and Ocean Science, Nanjing University, Nanjing, China, [6]Department of Earth System Sciences, Tsinghua University, Beijing, China, [7]College of Global Change and Earth System Science, Beijing Normal University, Beijing, China, [8]Henan Provincial Key Laboratory of Hydrosphere and Watershed Water Security, North China University of Water Resources and Electric Power, Zhengzhou, China

Abstract Tropical cyclone precipitation (TCP) and associated floods have caused widespread damage globally. Despite growing evidence of significant changes in the activity of tropical cyclones (TCs) in recent decades, the influence of TCs on regional flooding remains poorly understood. Here, we distinguish the role of TCs in fluvial discharge by explicitly simulating discharge with and without observed TCP in the Lancang–Mekong River Basin, a vulnerable TC hotspot. Our results show that TCs typically contributed approximately 30% of annual maximum discharge during 1967–2015. However, for rare and high-magnitude floods (long return periods), TCs are the dominant driver of extreme discharge events. Moreover, spatial changes in TC-induced discharge are closely related to changes in TCP and TC tracks, showing increasing trends upstream but decreasing trends downstream. This study reveals significant spatiotemporal differences in TC-induced discharges and provides a methodology for quantifying the role of TCs in fluvial discharge.

Plain Language Summary Tropical cyclone (TC)-induced floods constitute a significant cause of life loss and property damage worldwide. Despite the proliferation of literature on flood dynamics, TC impacts on regional flooding in the Lancang–Mekong River Basin remain poorly quantified. To address this knowledge gap, we applied the widely used Variable Infiltration Capacity hydrological model to simulate daily discharge both with and without TC precipitation inputs in the active TC landfalling region. Our results demonstrate that TCs generate significantly higher discharge in downstream areas compared to upstream areas, contributing more than 30% of annual flood peaks at most stations from 1967 to 2015. TCs are the primary driver of high-magnitude floods with long return periods. Furthermore, the spatiotemporal changes in TC-induced discharge closely correspond to changes in TC characteristics. This study underscores the critical influence of TC activity on flood dynamics and demonstrates the growing importance of TCs in extreme floods.

1. Introduction

Tropical cyclones (TCs) are disastrous natural hazards that have caused major losses via associated floods (Brakenridge, 2019). Previous studies have found significant increasing trends in the TCs' intensity and rainfall rate, poleward movement of TC tracks, and changes in the seasonal cycles of intense TCs in the past decades (Knutson et al., 2019, 2020; Kossin et al., 2016; Utsumi & Kim, 2022). With more major storms making landfall (S. Wang & Toumi, 2021, 2022), the ongoing coastal migration faces increased exposure to TCs landfalling. In particular, the regional TC-induced discharge is a critical proxy of disastrous natural hazards and an essential factor influencing the regional hydroclimate (Chen et al., 2024; Gori et al., 2020; Stelly et al., 2024), ecosystems (Darby et al., 2016; Erban et al., 2014), and even the global food market (Chau et al., 2013; Mekong River Commission, 2010). However, assessing the risk of disastrous TC-induced floods requires a deeper understanding of how and to what extent the changes in TC activity can influence discharge due to the complex interactions between the variability of TC activity and watershed properties (Merz et al., 2021; Yang et al., 2020).

To address the question, we select the Lancang–Mekong River Basin (LMRB) as the study area, which suffers from one of the highest flood mortality rates on Earth (Figure 1a) (Bangalore et al., 2018; Ziegler et al., 2020). The TCs have claimed about a quarter of the flood occurrences in the Mekong region (Chen, Giese, et al., 2020). Some

Hao Huang, Long Yang, Deliang Chen, Bin He, Junguo Liu

recent studies have investigated compound flooding affected by TC precipitation and its interaction with storm surge, focusing mainly on the coast (Gori et al., 2020; Qiu et al., 2022). Most studies have only concentrated on the impact of TCs on extreme precipitation, leaving the direct connections between TCs and fluvial floods understudied (Chhin et al., 2016; Takahashi et al., 2015). With the intensified TCs in a warming climate, the LMRB is also projected to face increasing intensity of future TCs (Chen, Emanuel, et al., 2020; Tran, Ritchie, Perkins-Kirkpatrick et al., 2022). Hence, quantifying the impact of TCs on fluvial discharge in the LMRB could help better understand the physical processes of floods.

Existing studies used to identify floods associated with TCs when the hydrological station is within a certain threshold (e.g., 500 km) radius of the TC center during a time window of TC passage (e.g., day −3 to day +7) (Villarini & Smith, 2010; Yang et al., 2020; Zhu et al., 2015). However, antecedent discharge often influences TC-induced discharge, and in-situ measurements cannot identify the discharge induced by specific observed TC and nonTC components. Therefore, basin-wide hydrological modeling using a holistic and explicit discharge simulation forced with scenarios differentiated by the presence of TC precipitation has been used to attribute the TC-induced discharge (Darby et al., 2016; Stelly et al., 2024).

The present study employed the macroscale Variable Infiltration Capacity (VIC) hydrological model (Liang et al., 1994) to simulate the daily discharge forced with two scenarios (one with and the other without observed TC precipitation (TCP) of the LMRB for 1967–2015 (Figure S1 in Supporting Information S1), and obtained the daily discharges induced from daily precipitation (P) and daily nonTC precipitation (nonTCP), abbreviated as Discharge and nonTC-Discharge, respectively (Figure S2 in Supporting Information S1). The daily TCP-induced discharge (TC-Discharge) was then derived for further analysis. Our study enables a physical process-based investigation of both TC and nonTC's influence on fluvial discharge across the basin, providing considerable advances in understanding changes in Mekong hydrology, especially the impacts of observed TCs.

2. Materials and Methods

2.1. Materials

Observed TC data were obtained from the latest International Best Track Archive for Climate Stewardship (IBTrACS) version 4, which records TC tracks every 3 hours (Knapp et al., 2010). From 1967 to 2015, 311 TCs affected the LMRB. Daily discharge observations (1961–2015) from eight hydrological stations on the LMRB's main stem were obtained from Mohammed et al. (2018) and the Mekong River Commission. These stations are within the TC-affected region (Figure 1a) (Chen et al., 2019; Darby et al., 2016). Gridded daily precipitation data were obtained from the widely used Asian Precipitation–Highly-resolved Observational Data Integration Toward the Evaluation of Water Resources database (0.25° × 0.25°) (Yatagai et al., 2012), providing a long-term daily product with satisfactory accuracy for the LMRB (Chen et al., 2018). Furthermore, its efficacy in simulating discharge has been demonstrated in the Mekong (Lauri et al., 2014; J. Wang et al., 2021). Temperature and wind speed (0.25° × 0.25°) were derived from the CN05.1 database (Wu & Gao, 2013) and the Princeton University Global Meteorological Forcing data set (Sheffield et al., 2006). Additional data, including soil parameters (250 m × 250 m), land use data (1 km × 1 km) and topography (10 × 10), were obtained from Global Soil Data Task (2014), Hansen et al. (2000), and Fujisada et al. (2011), respectively. These input data are critical for modeling the evapotranspiration, snowmelt, and soil moisture dynamics that underlie the VIC model's water and energy balance. They were processed as a 0.25° × 0.25° grid for input to the VIC model.

2.2. Model Calibration and Validation

Among existing hydrological models, the VIC model is particularly suitable for long-term basin-scale hydrological modeling, which is based on the Soil Vegetation Atmospheric Transfer (SVAT) scheme to simulate land-atmospheric fluxes, and the water and energy balances for each grid at the land surface, and a separate routing model is coupled to route estimated surface flows and base flows to produce discharge at the watershed outlets (Liang et al., 1994; Lohmann et al., 1996, 1998). The VIC model has been widely applied to major river basins globally, and it has proven effective in capturing daily discharge and floods in the LMRB (Hamman et al., 2018; J. Wang et al., 2021; Yun et al., 2020).

The model's spin-up, calibration, and validation periods were 1961–1966, 1967–1991, and 1992–2007, respectively. The validation period was limited to 2007 due to a lack of reservoir components and increased dam

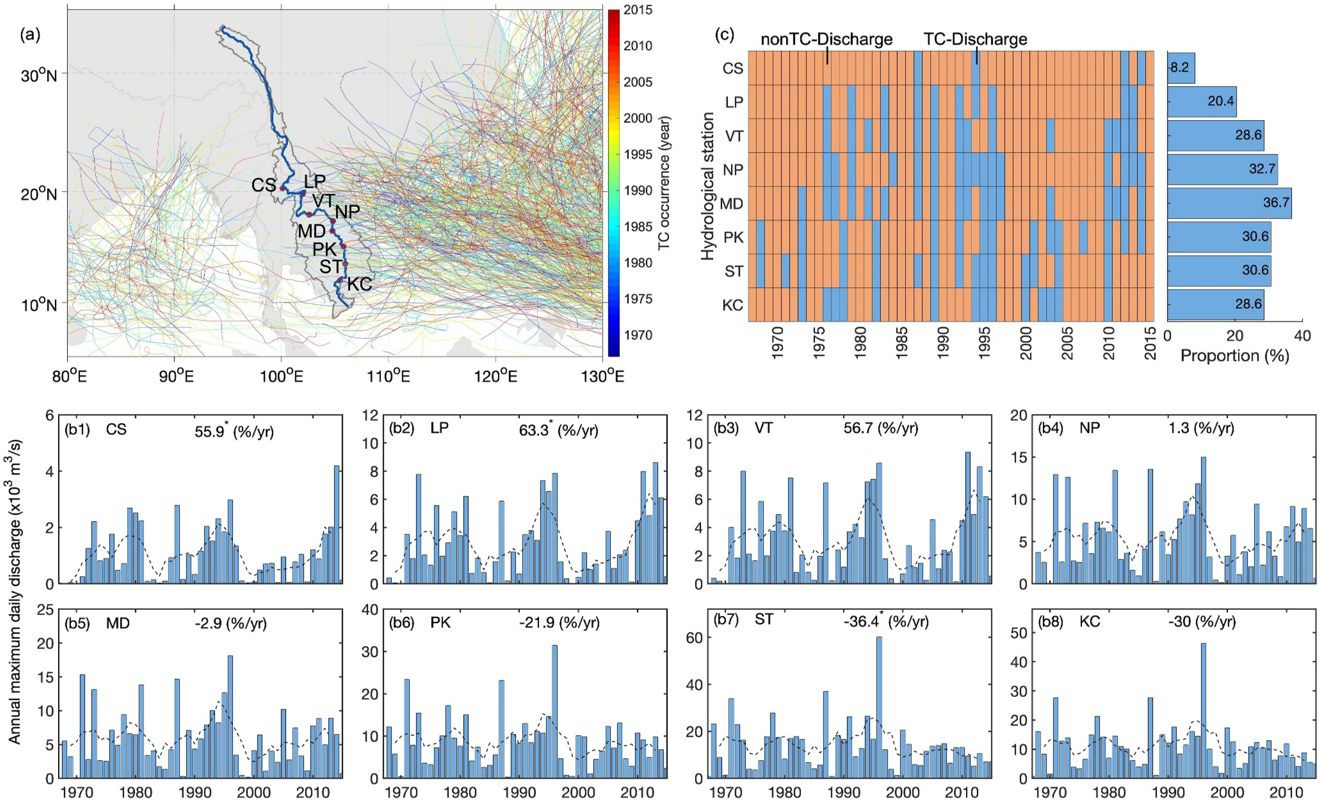

Figure 1. Annual maximum TC-Discharge of 1967–2015 at the eight hydrological stations in the LMRB. (a) TC track and the year of occurrence, (b) VIC-simulated annual maximum TC-Discharge in respective stations, and (c) annual distribution and proportions of annual maximum peaks associated with TC-Discharge. Hydrological stations of the river: Chiang Sean (CS), Luang Prabang (LP), Vientiane (VT), Nakhon Phanom (NP), Mukdahan (MD), Pakse (PK), Stung Treng (ST), and Kompong Cham (KC). In panel (b) the bars are the annual time series of the TC-Discharge, and the corresponding dashed lines are the 5-year moving average; the temporal trend of the annual time series is shown in black font and the asterisk indicates a trend above the 90% significance level. In panel (c) the percentage on the right of each horizontal bar displays the proportion of annual maximum peaks associated with TC-Discharge to Discharge during the period at each station.

constructions thereafter (see J. Wang et al. (2021) for details). The VIC model effectively simulated daily discharge in the LMRB in both annual and TC seasons (June–November), showing high Nash–Sutcliffe Efficiency coefficients (NSE) and Pearson correlation coefficients (Corr) across all stations during calibration and validation (Figure S3, Table S1, and S2 in Supporting Information S1). It also captured interannual fluctuations in annual maximum daily discharge, though it underestimated peak values (Figure S4 and Table S3 in Supporting Information S1).

Importantly, our methodology of derivation isolates TC's impact on fluvial discharge by simulating the difference between Discharge and nonTC-Discharge components, revealing the spatiotemporal changes of TC-Discharge. It serves our purpose of investigating the influence of TC on fluvial discharge. This framework has proven effective in simulating rainy season hydrology with low relative error and high NSE (over 0.9) (J. Wang et al., 2021), making it suitable for analyzing the impact of TCs on fluvial discharge in the LMRB.

2.3. Simulation and Extraction of TC-Induced Discharge

The 3-hourly TC track data were linearly interpolated to daily intervals to align with the temporal resolution of discharge observations. The methodology for simulating and extracting TC-induced discharge is as follows (Figure S1 in Supporting Information S1):

1. Gridded daily precipitation data from the APHRODITE was used to derive daily precipitation (P), daily TC precipitation (TCP), and daily nonTCP. The P is daily precipitation directly obtained from the APHRODITE data. The TCP is precipitation occurring at grids within the size of TCP along the TC tracks. Here, the size of TCP is defined as a conventional threshold of 500-km radius around TC center and 1 day before and after the

passage of a TC (e.g., Chen et al., 2019; Jiang & Zipser, 2010; Zhang et al., 2018), as most of the TCP occurs within a radius of 500 km (Khouakhi et al., 2017) and precipitation radius is largely independent of storm intensity (Lin et al., 2015). Precipitation outside the radius is classified as nonTCP. We obtained gridded binary values at $0.25° \times 0.25°$ resolution for 1961–2015 as a nonTCP and TCP occurrence date matrix with this definition. Using this occurrence date matrix as a mask for the daily gridded P data set, we obtained the corresponding gridded daily precipitation as nonTCP and TCP. Both daily P and nonTCP were then used as forcing inputs for discharge simulations.

2. Two sets of daily precipitation forcing were used to drive the VIC hydrological model. First, daily P forcing was used to simulate discharge with the combined influence of both TCP and nonTCP (Discharge). Then, daily nonTCP forcing was used to simulate discharge unaffected by TCs (nonTC-Discharge). The initial state of the model was kept consistent for simulating both Discharge and nonTC-Discharge. The difference between Discharge and nonTC-Discharge components was thus treated as caused by the observed TCs, referred to as TC-Discharge. This approach aligns with the methodology described by Darby et al. (2016), which yielded TC-Discharge for the eight hydrological stations (see examples in Figure S2 in Supporting Information S1). It is important to note that the simulated discharge components do not explicitly decompose the discharge of specific precipitation events. Instead, they reflect the cumulative effects of multiple precipitation events over an extended period (Darby et al., 2016).
3. To estimate TC's influence on fluvial discharge, we first obtained the annual maximum peaks of Discharge, nonTC-Discharge, and TC-Discharge at the eight hydrological stations, respectively. Then we associated an annual maximum peak of Discharge with a TC event at each station when it meets the following conditions: (a) if their annual maximum peaks coincided on the same day; or (b) if the TC-Discharge peak occurred before the Discharge peak, and the nonTC-Discharge peak occurred earlier than TC-Discharge or later than Discharge; or (c) if the first two conditions were not met, the annual maximum peak of Discharge was associated with nonTC-Discharge. Hence, we derived a time series of annual maximum peaks associated with TC-Discharge and nonTC-Discharge. The relative proportion of TC-discharge-associated peaks to the total number of annual maximum peaks (49 for 1967–2015) was calculated for each station. Our analysis focuses on the annual maximum TC-Discharge and its proportion to the annual maximum Discharge during the study period.

2.4. Extreme Value Analysis

To further estimate the potential impact of TC-Discharge on extreme floods, the return period of extreme discharge was evaluated by employing the widely used Generalized Extreme Value (GEV) distributions (Cole, 2001; van der Wiel et al., 2017). The GEV method was applied to the annual maximum Discharge, nonTC-Discharge, and TC-Discharge, respectively, to assess the extreme discharges. To account for uncertainty, we used the bootstrapping technique with 1000 iterations to estimate confidence intervals (Efron, 2003). The results demonstrated good fits to the annual maximum daily discharge of the fitted GEV cumulative distribution function (CDF) and the empirical CDF (Figure S5 in Supporting Information S1). Subsequently, utilizing the curve shape of the return level and return period of Discharge, nonTC-Discharge, and TC-Discharge, we estimated the probability of extreme flood occurrence and compared the potential influence between TC-Discharge and nonTC-Discharge.

2.5. Annual Extreme TCP and TC Track Density Analysis

Strong and long-lasting TCP is more likely to cause extreme floods (Yang et al., 2020). Thus, investigating the spatial patterns of TCP and TC track density enhances the understanding of spatiotemporal changes in TC-induced floods. We employed the estimated annual maximum daily TCP as extreme TCP. For the 3-hourly reported TC track from the IBTrACS, we calculated the annual track density by counting the TC track positions every 3 hours at the $1° \times 1°$ grid box, as the TC's translation speed ranging between ~5 and ~40 km/hr (Song et al., 2024). Then we applied a nine-point weighted smoother at each grid to the TC track density for better spatial continuity (W. Wang et al., 2010). During the study period, at each grid, an analysis was conducted of the mean and trend of the annual extreme TCP in the LMRB, as well as the mean and trend of the TC track density in the surrounding regions (85°E−125°E, 3°N–33°N).

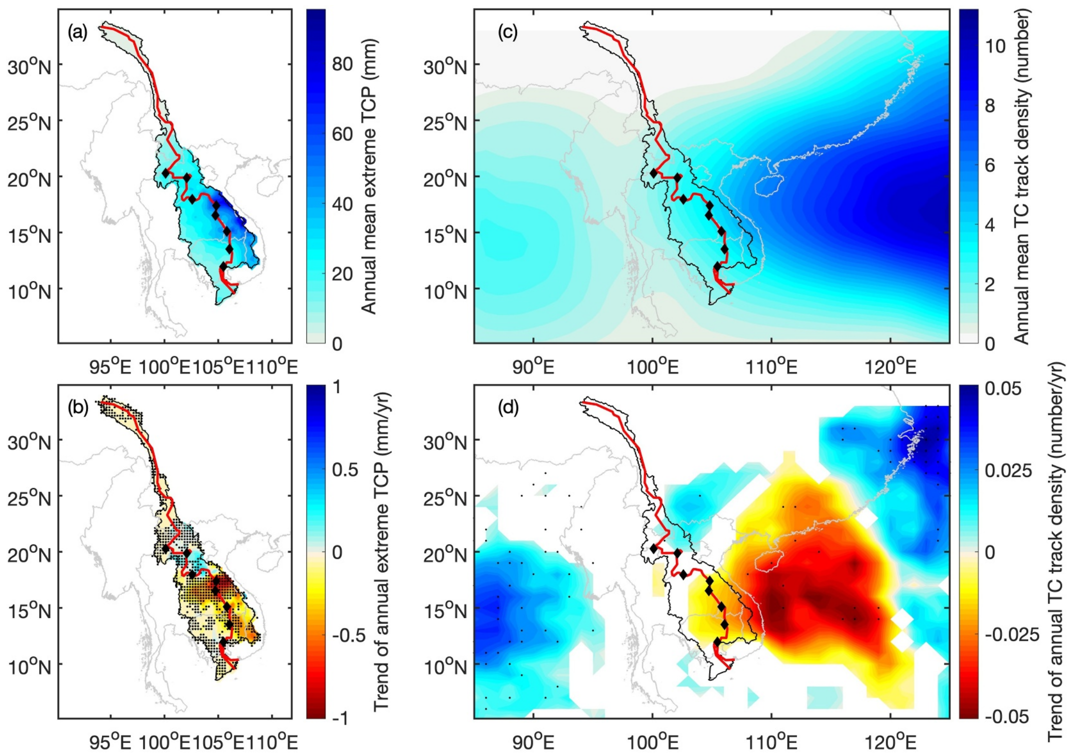

Figure 2. Spatial patterns in the annual mean and trend of the maximum daily TCP in the LMRB and the TC track density in the surrounding areas from 1967 to 2015: (a) annual mean and (b) trend of extreme TCP; (c) annual mean and (d) trend of TC track density. A black dot indicates a trend above the 95% significance level.

2.6. Trend Analysis

The non-parametric Sen's slope (Sen, 1968) and Mann–Kendall (Kendall, 1938) methods were employed to detect monotonic trends in discharge and precipitation from 1967 to 2015. These methods are widely used in hydro-climatic time series because they do not assume a normal data distribution and are less sensitive to extreme values than other trend detection methods (Chen et al., 2018; Tran, Ritchie, & Perkins-Kirkpatrick, 2022). To minimize the effect of the large interannual variability, we applied a 5-year moving average to the annual time series in the trend analysis (Emanuel, 2005).

3. Results and Discussion

3.1. Spatial Heterogeneity of Annual Maximum TC-Induced Discharge

The annual maximum TC-Discharge time series shows strong interannual fluctuations at the eight stations and share similar peaks and troughs, with the amount generally increasing from the CS to the ST station and then decreasing further downstream at the KC station (Figure 1b). However, the role of TCs in discharge generation is more significant downstream than upstream. For instance, TCs contribute to annual maximum discharge ranging from ∼400 to ∼4,000 m^3/s at the CS station and ∼800–∼6,000 m^3/s at the ST station.

TC-Discharge's spatial pattern aligns with TCP's regional spatial distribution (Darby et al., 2016; Tang et al., 2023), which is one of the most notable factors affecting floods (Kundzewicz et al., 2012; Yang et al., 2020). The extreme TCP is spatially heterogeneous (Figure 2). The lower eastern area of the LMRB experiences the highest levels of TCP, receiving a higher TC track density than other basin areas. At the same time, TCs and TCP rarely occur north of the CS station. The TCP affecting the lower eastern area was primarily influenced by TCs from the Western North Pacific (WNP), followed by those from the South China Sea, while TCP associated with TCs from the Bay of Bengal was concentrated in the western LMRB (Chen et al., 2023).

10.1029/2024GL113199

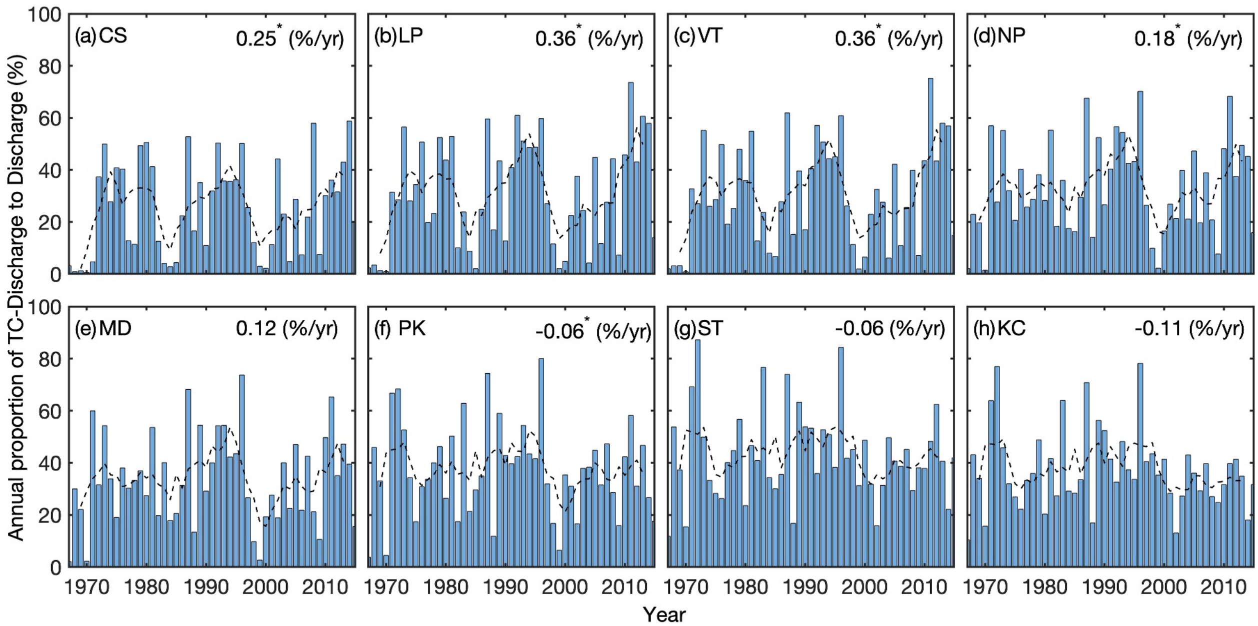

Figure 3. Percentages of annual maximum TC-Discharge to Discharge simulated by the VIC model during 1967–2015 at the eight hydrological stations within the LMRB. The bars are the proportion annual maximum time series of TC-Discharge, and the corresponding dashed black lines are the 5-year moving average, with the temporal trend shown in black font. An asterisk indicates a trend above the 90% significance level.

Along with the regional spatial distribution of TCP, TCs had more pronounced impacts on discharge downstream of the lower LMRB than they did upstream. Meanwhile, the annual extreme P shows a substantial reducing tendency in the upper and lower basins, with the most rapid declines coinciding with the precipitation center in the lower east (Figure S6 in Supporting Information S1). In contrast, increasing trends are scattered in the middle and lower basins. The significant extreme TCP in the lower eastern basin is critical to regional flooding (Takahashi et al., 2015), implying the importance of TCP to extreme floods. By calculating the proportion of annual maximum TC-Discharge to Discharge, we found TCs could contribute to an average of 25.4%–43.0% of the annual maximum discharge from CS station to ST station (Figure 3). Meanwhile, the maximum levels of these annual proportions could reach between 58.8% and 87.2% for the stations, indicating the TC's potential of extreme contribution to annual maximum discharge (Figure 3). Accordingly, through the spatially varying TCP, TC-Discharge could play a substantial role in extreme discharge, which is an important factor in triggering floods.

To further investigate the potential influence of TC-Discharge on floods, we estimated the annual maximum discharge associated with TC-Discharge and nonTC-Discharge, respectively. Results showed that TC-Discharge is typically responsible for a median of 29.6% of the annual maximum discharge among the stations, and there is spatial heterogeneity along the main stem of LMRB (Figure 1c). The annual maximum discharge associated with TC-Discharge was more prominent downstream than upstream. For example, 8.2% of the annual maximum discharge was associated with TC-Discharge at the CS station; the number grew to beyond 36.7% at the MD station and remained above 30% at downstream stations (PK, ST, and KC). Given the average of 6.4 landfalling TCs (about 18 days) per year and ~2.5% contribution of TCP to TP (Chen et al., 2019), the results imply the substantial impact of TCs on floods.

Our analysis also shows that discharge is extremely geographically specific, controlled by a combination of local climate and physiography effects. This is supported by earlier findings in the WNP (Chen, Giese, et al., 2020; Lindersson et al., 2021). Despite the lower amounts of TC-Discharge at upstream stations, about 20%–28% of TCP-associated annual maximum discharges occurred at, for example, LP and VT stations (Figure 1c), suggesting the potential contribution from local physiography. Furthermore, this area is located between a mountain range with high water flow velocity and a floodplain with low water flow velocity; short-duration heavy precipitation induced by TCs can rapidly generate extreme discharge (Tang et al., 2023; J. Wang et al., 2021). In addition, the record-breaking annual maximum TC-Discharge after 2010 at the first three stations also indicates

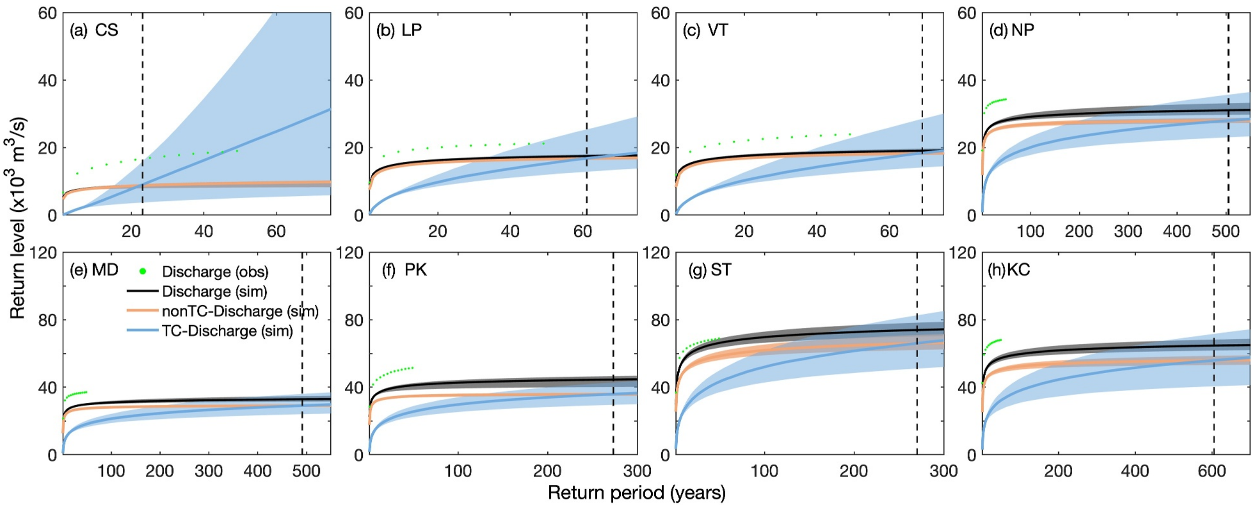

Figure 4. Return periods of the annual maximum discharge over the period 1967–2015 from Discharge (green, observations), Discharge (black, simulations), nonTC-Discharge (orange, simulations), and TC-Discharge (blue, simulations) at the eight hydrological stations within the LMRB fitting a Generalized Extreme Value (GEV) distribution. The upper and lower shading edges show the 25th- and 75th-percentiles, respectively, in return periods. The vertical black dash line marks the return period when the return level of TC-Discharge becomes greater than nonTC-Discharge.

the potential risk of TC-Discharge in the relatively few TCP occurring northern LMRB (Figures 1b and 2a), raising awareness of TC risk in the historically TC-scarce regions.

Utilizing the extensively employed GEV distributions (Cole, 2001; van der Wiel et al., 2017), we further disclose the impact of TC-Discharge on extreme floods (Figure 4). Due to relatively few TC landfalls, there is considerable uncertainty associated with TC-Discharge at the first station. For the remaining seven stations, the TC-Discharge's curve shape increases more pronouncedly at longer return periods compared to the nonTC-Discharge. Additionally, the observed data points indicate that the actual situation of extreme floods could be worse than our simulations. These findings collectively imply a heightened risk of extreme floods associated with TCs. A critical question is how much TCs contribute to extreme floods, which are pivotal for infrastructure design and flood defense planning. Figure 4 illustrates the return period at which TC-Discharge becomes the dominant driver of floods. The preponderant influence of TCs in upstream areas is evident in flood events with return periods larger than 20–70 years, and it becomes dominant in downstream flood events with return periods exceeding 200 years. While the initial return level of TC-Discharge is lower than that of nonTC-Discharge at shorter return periods, they eventually surpass nonTC-Discharge at longer return periods, particularly in downstream stations, irrespective of extrapolated values for long return periods. Overall, TCs are a major driver of extreme floods, though their impact on annual floods is minimal.

Extreme precipitation, a key driver of floods, can result from various weather types, including TCs and local monsoon systems (nonTC) (Lu et al., 2020). The LMRB's tropical monsoonal climate brings heavy precipitation during the monsoon season (June–October) (Räsänen & Kummu, 2013). TCs have been observed to induce precipitation peaks from September–November, significantly affecting regional flood dynamics (Chen et al., 2019; Mekong River Commission, 2010). Conventional flood frequency analysis assumes flood samples from the same population. However, our findings demonstrate the notable impact of TCs on extreme floods, challenging the assumption of homogeneity and enhancing our understanding of how different weather systems contribute to extreme floods.

3.2. The Spatiotemporal Trend of Annual Maximum TC-Induced Discharge

Trend analysis showed the regional distribution of the annual extreme TCP substantially declined in the lower basin and increased in a small area of the upper basin from 1967 to 2015 (Figure 2). Given the strong and highly significant coupling between TCP and TC track density (Chen et al., 2023), the spatiotemporal trend of TCP was due to the regional changes in TC track density, which was closely associated with the poleward shift of TC track in the WNP (Darby et al., 2016; Feng, 2024; Tran, Ritchie, & Perkins-Kirkpatrick, 2022). Meanwhile, annual maximum TC-Discharge presented contrasting trends between the upstream and downstream areas, with significant positive trends at the first two stations and negative trends at the penultimate stations (Figure 1). The contrasting trends of annual maximum TC-Discharge are closely associated with the changes in TCP and track density. Specifically, the station-wise trend analysis shows a significant linear relationship between the trend of annual TC track density and the trend of annual maximum TC-Discharge, with the first two upstream stations (CS and LP) exhibiting positive trends in both track density and TC-Discharge, while the downstream stations displaying negative trends (Figure S7 in Supporting Information S1). Additionally, the proportions of annual maximum TC-Discharge to Discharge displayed contrasting trends between upstream and downstream (Figure 3). Overall, the results highlight that spatial changes of TC-Discharge are closely aligned with changes in TC track and TCP, showing positive trends in upstream areas and negative trends in downstream areas.

Therefore, the WNP ocean-wide change of poleward TC activity has induced the regional inconsistency trends of TC-Discharge in the LMRB. If the poleward-shifting TC track continues under climate change (Kossin et al., 2016; Tran, Ritchie, Perkins-Kirkpatrick, et al., 2022), it will likely continue to influence the regional TC-Discharge. In addition, local changes in TC genesis in the South China Sea could also contribute to the decrease of TC track density in the south while slightly increasing in the north of the South China Sea (Park et al., 2014). Moreover, a decline in TC-Discharge could significantly reduce riverine suspended sediment transport, particularly in the subsiding mega-river deltas like the Mekong Delta, where sediment deposition is crucial for counteracting subsidence and sustaining regional stability in these “drowning” deltas (Darby et al., 2016).

Our study focused on quantifying the role of poleward shift of TC activity in influencing TCP and TC-Discharge. However, other factors, including changes in TC climatology (e.g., wind speed and storm size) and topography, also play a role (Cheung et al., 2018; Zhu et al., 2015). Future research should explore multiple TC-induced discharge peaks, incorporating the effect of TC climatology and topography under a changing climate, to improve understanding of the frequency and magnitude of extreme hydrological events. Moreover, in addition to acting as a hazard, TC-Discharge can serve as a valuable water resource to alleviate soil moisture deficits or be captured and stored in existing reservoirs (Maxwell et al., 2013). By distinguishing the role of TCs in fluvial discharge, this study provides a practicable methodology for future studies to quantify the contribution of TC-Discharge to both extreme floods and water resources under different scenarios.

4. Conclusions

Our study quantifies the influence of TCs on fluvial discharge and annual maximum peaks in the LMRB from 1967 to 2015 using the VIC hydrological model driven by forcings with and without TCP. The results demonstrate that TCs generate substantially higher extreme discharge downstream compared to upstream, attributable primarily to greater TCP and track density in the basin's lower eastern region. Furthermore, while TC-Discharge exhibits significant increasing trends at upstream stations, decreasing trends occur downstream during the period. For high-magnitude flood events, specifically those exceeding 50-year return periods upstream and 200-year return periods downstream, TCs emerge as the dominant flood driver. Our study presents the first modeling-based assessment of TC-induced fluvial floods in this active TC landfall region, revealing the profound influence of TCs on flood risk.

Acknowledgments
This work was supported by the National Natural Science Foundation of China (Grants 42361144001, 42101041), Guangdong Provincial Key Laboratory of Intelligent Disaster Prevention and Emergency Technologies for Urban Lifeline Engineering (2022) (Grant 2022B1212010016). It was also partly supported by the 111 project (Grant D25014), the National Foreign Experts Program (Category S) (Grant S20240116), and Henan Province Foreign Scientist Studio (Grant GZS2024013; 254000510004). D.C. was supported by the Swedish Research Council VR (2021-02163, 2022-06011). R.T. was supported by the Singapore Green Finance Centre.

Data Availability Statement

The data sets presented here can be found in the latest International Best Track Archive for Climate Stewardship (https://www.ncei.noaa.gov/data/international-best-track-archive-for-climate-stewardship-ibtracs/v04r00/access/netcdf/), the Asian Precipitation–Highly-resolved Observational Data Integration Towards Evaluation (APHRODITE v1101 and v1101EX_R1, https://search.diasjp.net/en/dataset/APHRO_MA) database, the Princeton hydrological data set (https://hydrology.soton.ac.uk/data/pgf/v3/0.25deg/daily/). Annual extreme discharge data are available at Chen (2025).

References

Bangalore, M., Smith, A., & Veldkamp, T. (2018). Exposure to floods, climate change, and poverty in Vietnam. *Economics of Disasters and Climate Change*, *3*(1), 79–99. https://doi.org/10.1007/s41885-018-0035-4

Brakenridge, G. R. (2019). Global active archive of large flood events. Retrieved from http://floodobservatory.colorado.edu/Archives/index.html

Chau, V. N., Holland, J., Cassells, S., & Tuohy, M. (2013). Using GIS to map impacts upon agriculture from extreme floods in Vietnam. *Applied Geography*, *41*, 65–74. https://doi.org/10.1016/j.apgeog.2013.03.014

Chen, A. (2025). Tropical cyclone precipitation induced fluvial discharge in the Lancang–Mekong River Basin [Dataset]. *figshare*. https://doi.org/10.6084/m9.figshare.28665872

Chen, A., Chen, D., & Azorin-Molina, C. (2018). Assessing reliability of precipitation data over the Mekong River Basin: A comparison of ground-based, satellite, and reanalysis datasets. *International Journal of Climatology*, *38*(11), 4314–4334. https://doi.org/10.1002/joc.5670

Chen, A., Emanuel, K. A., Chen, D., Lin, C., & Zhang, F. (2020). Rising future tropical cyclone-induced extreme winds in the Mekong River Basin. *Science Bulletin*, *65*(5), 419–424. https://doi.org/10.1016/j.scib.2019.11.022

Chen, A., Giese, M., & Chen, D. (2020). Flood impact on Mainland Southeast Asia between 1985 and 2018—The role of tropical cyclones. *Journal of Flood Risk Management*, *13*(2), e12598. https://doi.org/10.1111/jfr3.12598

Chen, A., Ho, C.-H., Chen, D., & Azorin-Molina, C. (2019). Tropical cyclone rainfall in the Mekong River Basin for 1983–2016. *Atmospheric Research*, *226*, 66–75. https://doi.org/10.1016/j.atmosres.2019.04.012

Chen, A., Huang, H., Wang, J., Li, Y., Chen, D., & Liu, J. (2023). An analysis of the spatial variation of tropical cyclone rainfall trends in Mainland Southeast Asia. *International Journal of Climatology*, *43*(13), 5912–5926. https://doi.org/10.1002/joc.8180

Chen, A., Pokhrel, Y., Chen, D., Huang, H., Dai, Z., He, B., et al. (2024). Impact of tropical cyclones and socioeconomic exposure on flood risk distribution in the Mekong Basin. *Communications Earth & Environment*, *5*(1), 704. https://doi.org/10.1038/s43247-024-01868-9

Cheung, K., Yu, Z., Elsberry, R. L., Bell, M., Jiang, H., Lee, T.-C., et al. (2018). Recent advance in research and forecasting of tropical cyclone rainfall. *Tropical Cyclone Research and Review*, *7*(2), 106–127.

Chhin, R., Trilaksono, N. J., & Hadi, T. W. (2016). Tropical cyclone rainfall structure affecting Indochina Peninsula and Lower Mekong River Basin (LMB). *Journal of Physics: Conference Series*, *739*, 012103. https://doi.org/10.1088/1742-6596/739/1/012103

Cole, S. (2001). *An introduction to statistical modeling of extreme values*. Springer Series in Statistics.

Darby, S. E., Hackney, C. R., Leyland, J., Kummu, M., Lauri, H., Parsons, D. R., et al. (2016). Fluvial sediment supply to a mega-delta reduced by shifting tropical-cyclone activity. *Nature*, *539*(7628), 276–279. https://doi.org/10.1038/nature19809

Efron, B. (2003). Second thoughts on the bootstrap. *Statistical Science*, *18*(2). https://doi.org/10.1214/ss/1063994968

Emanuel, K. A. (2005). Increasing destructiveness of tropical cyclones over the past 30 years. *Nature*, *436*(7051), 686–688. https://doi.org/10.1038/nature03906

Erban, L. E., Gorelick, S. M., & Zebker, H. A. (2014). Groundwater extraction, land subsidence, and sea level rise in the Mekong Delta, Vietnam. *Environmental Research Letters*, *9*(8), 084010. https://doi.org/10.1088/1748-9326/9/8/084010

Feng, X. (2024). Translation speed slowdown and poleward migration of Western North Pacific tropical cyclones. *npj Climate and Atmospheric Science*, *7*(1), 196. https://doi.org/10.1038/s41612-024-00748-5

Fujisada, H., Urai, M., & Iwasaki, A. (2011). Advanced methodology for ASTER DEM generation. *IEEE IEEE Transactions on Geoscience and Remote Sensing*, *49*(12), 5080–5091. https://doi.org/10.1109/tgrs.2011.2158223

Global Soil Data Task. (2014). Global soil data products CD-ROM contents (IGBP-DIS) [Dataset]. *Global Soil Data Task*. https://doi.org/10.3334/ORNLDAAC/565

Gori, A., Lin, N., & Smith, J. (2020). Assessing compound flooding from landfalling tropical cyclones on the North Carolina Coast. *Water Resources Research*, *56*(4), e2019WR026788. https://doi.org/10.1029/2019wr026788

Hamman, J. J., Nijssen, B., Bohn, T. J., Gergel, D. R., & Mao, Y. (2018). The Variable Infiltration Capacity model version 5 (VIC-5): Infrastructure improvements for new applications and reproducibility. *Geoscientific Model Development*, *11*(8), 3481–3496. https://doi.org/10.5194/gmd-11-3481-2018

Hansen, M. C., Defries, R. S., Townshend, J. R. G., & Sohlberg, R. (2000). Global land cover classification at 1 km spatial resolution using a classification tree approach. *International Journal of Remote Sensing*, *21*(6–7), 1331–1364. https://doi.org/10.1080/014311600210209

Jiang, H., & Zipser, E. J. (2010). Contribution of tropical cyclones to the global precipitation from eight seasons of TRMM data: Regional, seasonal, and interannual variations. *Journal of Climate*, *23*(6), 1526–1543. https://doi.org/10.1175/2009jcli3303.1

Kendall, M. G. (1938). A new measure of rank correlation. *Biometrika*, *30*(1–2), 81–93. https://doi.org/10.1093/biomet/30.1-2.81

Khouakhi, A., Villarini, G., & Vecchi, G. A. (2017). Contribution of tropical cyclones to rainfall at the global scale. *Journal of Climate*, *30*(1), 359–372. https://doi.org/10.1175/jcli-d-16-0298.1

Knapp, K. R., Kruk, M. C., Levinson, D. H., Diamond, H. J., & Neumann, C. J. (2010). The International Best Track Archive for Climate Stewardship (IBTrACS). *Bulletin of the American Meteorological Society*, *91*(3), 363–376. https://doi.org/10.1175/2009bams2755.1

Knutson, T., Camargo, S. J., Chan, J. C. L., Emanuel, K., Ho, C.-H., Kossin, J., et al. (2019). Tropical cyclones and climate change assessment: Part I: Detection and attribution. *Bulletin of the American Meteorological Society*, *100*(10), 1987–2007. https://doi.org/10.1175/bams-d-18-0189.1

Knutson, T., Camargo, S. J., Chan, J. C. L., Emanuel, K., Ho, C.-H., Kossin, J., et al. (2020). Tropical cyclones and climate change assessment: Part II: Projected response to anthropogenic warming. *Bulletin of the American Meteorological Society*, *101*(3), E303–E322. https://doi.org/10.1175/bams-d-18-0194.1

Kossin, J. P., Emanuel, K. A., & Camargo, S. J. (2016). Past and projected changes in Western North Pacific tropical cyclone exposure. *Journal of Climate*, *29*(16), 5725–5739. https://doi.org/10.1175/jcli-d-16-0076.1

Kundzewicz, Z. W., Kanae, S., Seneviratne, S. I., Handmer, J., Nicholls, N., Peduzzi, P., et al. (2012). Flood risk and climate change: Global and regional perspectives. *Hydrological Sciences Journal*, *59*(1), 1–28. https://doi.org/10.1080/02626667.2013.857411

Lauri, H., Räsänen, T. A., & Kummu, M. (2014). Using reanalysis and remotely sensed temperature and precipitation data for hydrological modeling in monsoon climate: Mekong river case study. *Journal of Hydrometeorology*, *15*(4), 1532–1545. https://doi.org/10.1175/jhm-d-13-084.1

Liang, X., Lettenmaier, D. P., Wood, E. F., & Burges, S. J. (1994). A simple hydrologically based model of land surface water and energy fluxes for general circulation models. *Journal of Geophysical Research*, *99*(D7), 14415–14428. https://doi.org/10.1029/94jd00483

Lin, Y., Zhao, M., & Zhang, M. (2015). Tropical cyclone rainfall area controlled by relative sea surface temperature. *Nature Communications*, *6*(1), 6591. https://doi.org/10.1038/ncomms7591

Lindersson, S., Brandimarte, L., Mård, J., & Di Baldassarre, G. (2021). Global riverine flood risk—How do hydrogeomorphic floodplain maps compare to flood hazard maps? *Natural Hazards and Earth System Sciences*, *21*(10), 2921–2948. https://doi.org/10.5194/nhess-21-2921-2021

Lohmann, D., Nolte-Holube, R., & Raschke, E. (1996). A large-scale horizontal routing model to be coupled to land surface parametrization schemes. *Tellus*, *48*(5), 708–721. https://doi.org/10.1034/j.1600-0870.1996.t01-3-00009.x

Lohmann, D., Raschke, E., Nijssen, B., & Lettenmaier, D. P. (1998). Regional scale hydrology: I. Formulation of the VIC-2L model coupled to a routing model. *Hydrological Sciences Journal*, *43*(1), 131–141. https://doi.org/10.1080/02626669809492107

Lu, W., Lei, H., Yang, W., Yang, J., & Yang, D. (2020). Comparison of floods driven by tropical cyclones and monsoons in the southeastern coastal region of China. *Journal of Hydrometeorology*, *21*(7), 1589–1603. https://doi.org/10.1175/jhm-d-20-0002.1

Maxwell, J. T., Ortegren, J. T., Knapp, P. A., & Soulé, P. T. (2013). Tropical cyclones and drought amelioration in the Gulf and southeastern coastal United States. *Journal of Climate*, *26*(21), 8440–8452. https://doi.org/10.1175/jcli-d-12-00824.1

Mekong River Commission. (2010). State of the basin report 2010. Retrieved from https://www.mrcmekong.org/assets/Publications/basin-reports/MRC-SOB-report-2010full-report.pdf

Merz, B., Blöschl, G., Vorogushyn, S., Dottori, F., Aerts, J. C. J. H., Bates, P., et al. (2021). Causes, impacts and patterns of disastrous river floods. *Nature Reviews Earth & Environment*, *2*(9), 592–609. https://doi.org/10.1038/s43017-021-00195-3

Mohammed, I. N., Bolten, J. D., Srinivasan, R., & Lakshmi, V. (2018). Satellite observations and modeling to understand the Lower Mekong River basin streamflow variability. *Journal of Hydrology*, *564*, 559–573. https://doi.org/10.1016/j.jhydrol.2018.07.030

Park, D.-S. R., Ho, C.-H., & Kim, J.-H. (2014). Growing threat of intense tropical cyclones to East Asia over the period 1977–2010. *Environmental Research Letters*, *9*(1), 014008. https://doi.org/10.1088/1748-9326/9/1/014008

Qiu, J., Liu, B., Yang, F., Wang, X., & He, X. (2022). Quantitative stress test of compound coastal-fluvial floods in China's Pearl River delta. *Earth's Future*, *10*(5). https://doi.org/10.1029/2021ef002638

Räsänen, T. A., & Kummu, M. (2013). Spatiotemporal influences of ENSO on precipitation and flood pulse in the Mekong River Basin. *Journal of Hydrology*, *476*, 154–168. https://doi.org/10.1016/j.jhydrol.2012.10.028

Sen, P. K. (1968). Estimates of the regression coefficient based on Kendall's Tau. *Journal of the American Statistical Association*, *63*(324), 1379–1389. https://doi.org/10.2307/2285891

Sheffield, J., Goteti, G., & Wood, E. F. (2006). Development of a 50-year high-resolution global dataset of meteorological forcings for land surface modeling. *Journal of Climate*, *19*(13), 3087–3111. https://doi.org/10.1175/jcli3790.1

Song, J., Klotzbach, P. J., Dai, Y., & Duan, Y. (2024). A slowdown in translation speed of Western North Pacific tropical cyclones undergoing rapid intensification. *Geophysical Research Letters*, *51*(18). https://doi.org/10.1029/2024gl110220

Stelly, J., Pokhrel, Y., Tiwari, A. D., Dang, H., Lo, M.-H., Yamazaki, D., & Lee, T.-Y. (2024). Reconstruction of long-term hydrologic change and typhoon-induced flood events over the entire island of Taiwan. *Journal of Hydrology: Regional Studies*, *53*, 101806. https://doi.org/10.1016/j.ejrh.2024.101806

Takahashi, H. G., Fujinami, H., Yasunari, T., Matsumoto, J., & Baimoung, S. (2015). Role of tropical cyclones along the monsoon trough in the 2011 Thai flood and interannual variability. *Journal of Climate*, *28*(4), 1465–1476. https://doi.org/10.1175/jcli-d-14-00147.1

Tang, R., Dai, Z., Mei, X., Zhou, X., Long, C., & Van, C. M. (2023). Secular trend in water discharge transport in the Lower Mekong River-delta: Effects of multiple anthropogenic stressors, rainfall, and tropical cyclones. *Estuarine, Coastal and Shelf Science*, *281*, 108217. https://doi.org/10.1016/j.ecss.2023.108217

Tran, T. L., Ritchie, E. A., & Perkins-Kirkpatrick, S. E. (2022). A 50-year tropical cyclone exposure climatology in Southeast Asia. *Journal of Geophysical Research: Atmospheres*, *127*(4), e2021JD036301. https://doi.org/10.1029/2021jd036301

Tran, T. L., Ritchie, E. A., Perkins-Kirkpatrick, S. E., Bui, H., & Luong, T. M. (2022). Future changes in tropical cyclone exposure and impacts in Southeast Asia from CMIP6 Pseudo-global warming simulations. *Earth's Future*, *10*(12), e2022EF003118. https://doi.org/10.1029/2022ef003118

Utsumi, N., & Kim, H. (2022). Observed influence of anthropogenic climate change on tropical cyclone heavy rainfall. *Nature Climate Change*, *12*(5), 436–440. https://doi.org/10.1038/s41558-022-01344-2

van der Wiel, K., Kapnick, S. B., van Oldenborgh, G. J., Whan, K., Philip, S., Vecchi, G. A., et al. (2017). Rapid attribution of the August 2016 flood-inducing extreme precipitation in south Louisiana to climate change. *Hydrology and Earth System Sciences*, *21*(2), 897–921. https://doi.org/10.5194/hess-21-897-2017

Villarini, G., & Smith, J. A. (2010). Flood peak distributions for the eastern United States. *Water Resources Research*, *46*(6), W06504. https://doi.org/10.1029/2009wr008395

Wang, B., Yang, Y., Ding, Q.-H., Murakami, H., & Huang, F. (2010). Climate control of the global tropical storm days (1965–2008). *Geophysical Research Letters*, *37*(7), L07704. https://doi.org/10.1029/2010gl042487

Wang, J., Yun, X., Pokhrel, Y., Yamazaki, D., Zhao, Q., Chen, A., & Tang, Q. (2021). Modeling daily floods in the Lancang-Mekong River basin using an improved hydrological-hydrodynamic model. *Water Resources Research*, *57*, e2021WR029734. https://doi.org/10.1029/2021WR029734

Wang, S., & Toumi, R. (2021). Recent migration of tropical cyclones toward coasts. *Science*, *371*(6528), 514–517. https://doi.org/10.1126/science.abb9038

Wang, S., & Toumi, R. (2022). More tropical cyclones are striking coasts with major intensities at landfall. *Scientific Reports*, *12*(1), 5236. https://doi.org/10.1038/s41598-022-09287-6

Wu, J., & Gao, X. J. (2013). A gridded daily observation dataset over China region and comparison with the other datasets. *Chinese Journal of Geophysics*, *56*(4), 1102–1111.

Yang, L., Villarini, G., Zeng, Z., Smith, J., Liu, M., Li, X., et al. (2020). Riverine flooding and landfalling tropical cyclones over China. *Earth's Future*, *8*(3), e2019EF001451. https://doi.org/10.1029/2019ef001451

Yatagai, A., Kamiguchi, K., Arakawa, O., Hamada, A., Yasutomi, N., & Kitoh, A. (2012). APHRODITE: Constructing a long-term daily gridded precipitation dataset for Asia based on a dense network of rain Gauges. *Bulletin of the American Meteorological Society*, *93*(9), 1401–1415. https://doi.org/10.1175/bams-d-11-00122.1

Yun, X., Tang, Q., Wang, J., Liu, X., Zhang, Y., Lu, H., et al. (2020). Impacts of climate change and reservoir operation on streamflow and flood characteristics in the Lancang-Mekong River Basin. *Journal of Hydrology*, *590*, 125472. https://doi.org/10.1016/j.jhydrol.2020.125472

Zhang, Q., Lai, Y., Gu, X., Shi, P., & Singh, V. P. (2018). Tropical cyclonic rainfall in China: Changing properties, seasonality, and causes. *Journal of Geophysical Research: Atmospheres*, *123*(9), 4476–4489. https://doi.org/10.1029/2017jd028119

Zhu, L., Quiring, S. M., Guneralp, I., & Peacock, W. G. (2015). Variations in tropical cyclone-related discharge in four watersheds near Houston, Texas. *Climate Risk Management*, *7*, 1–10. https://doi.org/10.1016/j.crm.2015.01.002

Ziegler, A. D., Lim, H. S., Wasson, R. J., & Williamson, F. C. (2020). Flood mortality in SE Asia: Can palaeo-historical information help save lives? *Hydrological Processes*, *35*(1), e13989. https://doi.org/10.1002/hyp.13989